PAPER

Check for updates

A 2-chloroethyl ethyl sulfide (2-CEES) gas sensor based on a WO₃/graphite nanocomposite with high selectivity and fast response-recovery properties†

Chenguang Qiu,[a] Kun Li,[a] Wenlong Yan,[ab] Yong Fan,[b] Changyue Xia,[b] Chuang Sun,[b] Wei Zeng [ID] [ab] and Siliang Wang [ID] ★[ab]

Sensitive detection of toxic and harmful gases is essential in the field of environmental monitoring and human health. Among the detection strategies, gas sensors based on metal oxides are widely adopted. However, the gas sensor based on a single metal oxide has some problems such as poor selectivity and long response recovery time, which limit its further practical application. This paper is committed to improving the selectivity and shortening the response-recovery time toward 2-chloroethyl ethyl sulfide (2-CEES, dichlorodiethyl sulfide simulation). Tungsten oxide (WO₃)/graphite nanocomposites were prepared by simple blending, and the sensing performance toward 2-CEES gas was explored. The experimental results show that the WO₃/graphite gas sensor with a WO₃ mass fraction of 97% exhibits excellent sensing performance. In more detail, the device has a high response of 63% for 5.70 ppm 2-CEES at a working temperature of 260 °C, a fast response-recovery time (8 s/34 s) and high selectivity compared with ammonia, acetone, ethanol, and other toxic gas simulation gases [dimethyl methylphosphonate (DMMP) and acetonitrile]. This study provides an effective strategy to realize a high-performance gas sensor for dichlorodiethyl sulfide.

Introduction

Toxic and harmful gases existing in daily life can damage the human body. These agents are classified into blister agents, nerve agents, blood agents and pulmonary agents according to their toxic mechanism toward the human body.[1,2] Among them, the main representative of blister agents is dichlorodiethyl sulfide. Studies have shown that when the human body is exposed to an atmosphere of dichlorodiethyl sulfide, it can cause local damage to the skin, eyes, respiratory tract and other parts, and even in low concentrations of dichlorodiethyl sulfide, it will cause death.[3,4] Therefore, effectively detecting low concentrations of dichlorodiethyl sulfide has great importance in both environmental protection and human healthcare. At present, the detection of dichlorodiethyl sulfide mainly adopts

ion migration spectrometry, mass spectrometry, gas chromatography, micro-cantilever sensors, surface acoustic wave sensors, quartz-crystal microbalance sensors (QCMs), and fluorescence detection kits.[5–13] However, these techniques are complex, expensive, time-consuming to operate, and the accuracy of the equipment decreases due to aging.[14] By contrast, gas sensors based on metal oxide have the advantages of simple preparation, fast response speed and high sensitivity.[15–22]

Due to the great toxicity of toxic and harmful gases, it is very dangerous to directly use toxic and harmful gases for experiments in the laboratory. Therefore, simulants with physicochemical properties and structures similar to toxic and harmful gases are generally used for experiments, and the chemical gas 2-chloroethyl ethyl sulfide (2-CEES) is commonly used for dichlorodiethyl sulfide simulants.[23,24] In recent years, 2-CEES sensors based on metal oxides have been reported successively. For example, Pt-doped CdSnO₃ and Ru-doped CdSnO₃ nanostructured films prepared by ultrasonic spray pyrolysis were used to sense 2-CEES, and the results showed that the sensor has good detection ability, but the recovery time of this sensor for 2-CEES gas is too long.[24,25] Ran Yoo *et al.* investigated the sensing properties of ZnO nanoparticles and Al-doped ZnO nanoparticles for 2-CEES. The response of ZnO nanoparticles to 1 ppm 2-CEES at a temperature of 250 °C is 15, and the

[a] *East China Institute of Photo-Electron ICs, No. 89 Longshan Road, Suzhou 215163, Jiangsu Province, People's Republic of China. E-mail: sliang_wang@163.com*

[b] *Information Materials and Intelligent Sensing Laboratory of Anhui Province, Industry-Education-Research Institute of Advanced Materials and Technology for Integrated Circuits, Anhui University, No. 111 Jiulong Road, Hefei 230601, Anhui Province, People's Republic of China*

† Electronic supplementary information (ESI) available. See DOI: https://doi.org/10.1039/d2ma00621a

response of Al-doped ZnO nanoparticles to 20 ppm 2-CEES at a temperature of 500 °C is 954.2. Although ZnO-based sensors have good responses, they suffer from higher operating temperatures.[26]

Due to the poor sensor recovery ability and lack of selectivity in the above-mentioned literature, a gas sensor based on tungsten oxide (WO_3)/graphite composites was fabricated with a fast response-recovery time and excellent selectivity to 2-CEES gas in this paper. The gas sensor has a 63% response toward 5.70 ppm 2-CEES at a temperature of 260 °C, a rapid response/recovery time (8 s/34 s), and excellent reproducibility and long-term stability. It can detect a relatively low concentration of 2-CEES gas. The detection limit is 0.10 ppm, and the sensitivity is 22%. The response of the gas sensor to 2-CEES gas is almost 30 times higher than that of ammonia and acetonitrile at the same concentration, 10 times higher than that of ethanol, 5 times higher than that of DMMP, and 4 times higher than that of acetone, indicating that the sensor has good selectivity. This study provides an effective strategy for realizing a dichloro-diethyl sulfur gas sensor with high selectivity and a fast response recovery time.

Experimental methods

Chemical reagent

All chemicals used in this study were not further purified. Acetone (C_3H_6O), ammonia ($NH_3(aq)$), and ethanol (C_2H_5OH), were purchased from Sinopharm Chemical Reagent Co., Ltd. 2-Chloroethy ethyl sulfide (C_4H_9ClS), dimethyl methylphosphonate ($C_3H_9O_3P$), acetonitrile (C_2H_3N), and tungsten oxide (WO_3, average particle size <100 nm) were purchased from Shanghai Macklin Biochemical Co., Ltd. Deionized (DI) water was used in the whole experiment.

Materials synthesis

In a typical experiment, a given quantity of graphite was dispersed in ethanol/deionized water (volume fraction of 5:1) to obtain a uniform mixture (0.09 mg ml^{-1}). Afterwards, WO_3 nanopowders with various weights of 80 mg, 90 mg, 100 mg and 110 mg were respectively added into graphite solution (30 ml) under magnetic stirring for 24 h. Then, the mixed materials were put into an oven for 24 hours at a temperature of 60 °C, and were marked as S1, S2, S3 and S4, respectively.

Characterization

The morphology and structure of the sensing materials were characterized using a transmission electron microscope (TEM, JEM-2100), scanning electron microscopy (SEM, S-4800) and X-ray diffraction (XRD, SmartLab, 9 KW).

Measurements

The WS-30B gas sensor test system (Zhengzhou Weisheng Electronic Technology Co., Ltd) was used to test the sensor performance. The width of both gold electrodes on the ceramic tube is 0.6 mm, and the gap between the two gold electrodes is
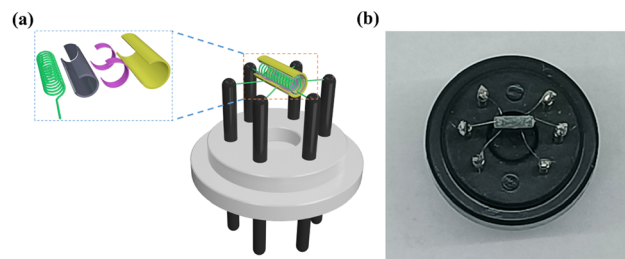

Fig. 1 The gas sensor used in the experiment. (a) Schematic diagram and (b) physical photo of the gas sensor.

1.0 mm. First, the sensing material was dispersed in agate mortar, mixed with an appropriate amount of deionized water, and ground to obtain a uniform slurry. The slurry was uniformly coated on the Al_2O_3 ceramic tube containing gold electrodes. Then the ceramic tube was put into the oven at a temperature of 180 °C for half an hour, to remove moisture. The ceramic tube was welded on a pedestal with six probes, and a Ni–Cr alloy coil was inserted into the tube, as shown in Fig. 1a. The working temperature can be controlled by adjusting the heating current flowing through the heater. An actual photo of the sensor is shown in Fig. 1b. The sensor is inserted into the measuring board of the sensor measurement system for gas sensing measurement. Inject a corresponding amount of liquid corresponding to a certain concentration calculated in advance through a micro syringe. A specific concentration of test gas can be obtained by heating and evaporating a corresponding amount of liquid. The corresponding amount of injected liquid is obtained from the following formula: $C = \dfrac{22.4 \times \varphi \times \rho \times V_1}{M \times V_2} \times 1000$, where C (ppm) is the target gas concentration, ρ (g mL^{-1}) is the density of the liquid, φ is the required gas volume fraction, V_1 (μL) is the volume of liquid, V_2 (L) is the volume of the chamber, and M (g mol^{-1}) is the molecular weight of the liquid. The resistance change is displayed in real time through the software on the computer. The sensor sensitivity formula is defined as S (%) = $(R_a - R_g)/R_a \times 100$, where R_a and R_g are the resistances in the air and in the test gas atmosphere, respectively. Gas response time and recovery time are defined as the time required for 90% of the total resistance change.

Results and discussion

Material characterizations

Firstly, the morphology and microstructure of raw materials and composites were studied. From Fig. 2a and Fig. S1a (ESI†), it can be seen that WO_3 is in the shape of nanoparticles. The high resolution TEM (HRTEM) indicates that the lattice spacing of WO_3 is 0.37 nm and the corresponding crystal plane is (020), as shown in Fig. 2b. The TEM and SEM images of graphite are shown in Fig. 2c and Fig. S1b (ESI†). From the figures, it can be seen that the graphite presents a multi-layer flake structure. Fig. 2d and Fig. S2 (ESI†) show the SEM images of WO_3/graphite composites with different mass ratios of WO_3 to graphite. The
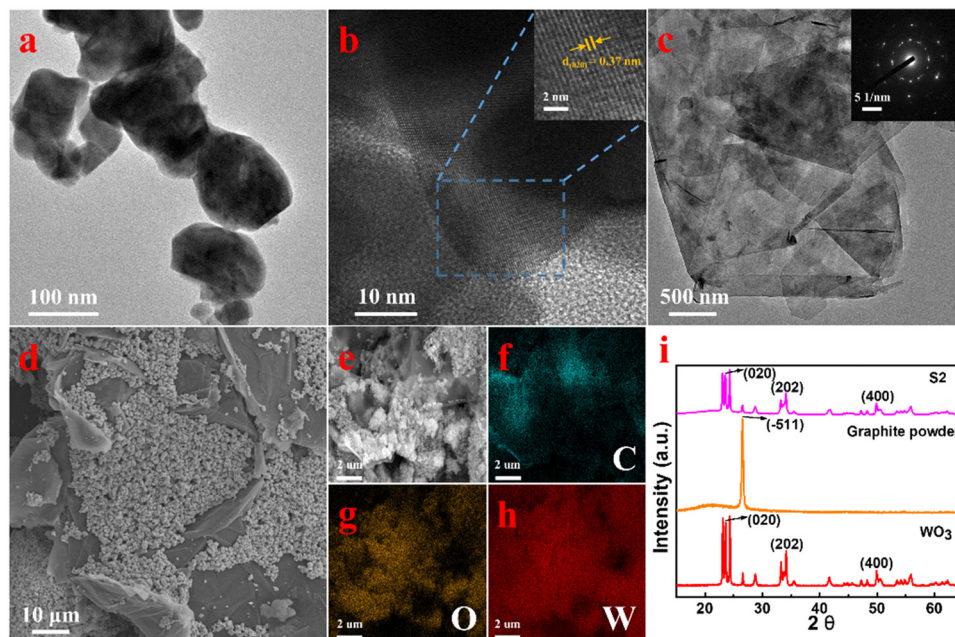
Fig. 2 Characterization of WO₃, graphite and WO₃/graphite. (a) TEM images of WO₃ nanoparticles. (b) HRTEM image of WO₃ nanoparticles. (c) TEM images of graphite. (d) SEM image of WO₃/graphite (S2). (e–h) elemental mapping images of WO₃/graphite (S2). (i) XRD patterns of WO₃, graphite and WO₃/graphite (S2).

WO₃ nanoparticles are firmly attached to the graphite sheet, and the WO₃ adheres and clusters together on the surface of graphite more and more with an increase of mass ratios. The composition of the S2 was further characterized using elemental mapping analyses, and the results are shown in Fig. 2(e–h). C, O and W elements were evenly dispersed in the whole product, confirming that the composites are composed of WO₃ and graphite without other impurities. The structure of S2 was further characterized by X-ray diffraction (XRD), as shown in Fig. 2i. The main diffraction peaks of S2 are located at angles of 23.6°, 34.2° and 49.9°, respectively, corresponding to the (020), (202) and (400) planes of WO₃ (JCPDS # 83-0950). The XRD results indicated that the incorporation of graphite did not cause any change in the crystalline phase of the WO₃ nanoparticles. In addition, no other diffraction peaks were observed, which indicates that the high purity of the synthetic powder was guaranteed by the high purity of raw materials and the cleanness of the synthesis process. The specific surface areas of the WO₃ and WO₃/graphite were, respectively, 5.3456 and 6.1215 m² g⁻¹ (Table 1).

Gas-sensing properties

The influence of the working temperature on the response of the sensors was first studied, as shown in Fig. 3a and Fig. S3

(ESI†). The concentration of the measured 2-CEES gas is 5.70 ppm. It can be seen that the S2 sensor had the highest response at all operating temperatures. The response of S1, S3 and S4 sensors at all operating temperatures is relatively small, no more than 30%. This is because with the gradual addition of WO₃ concentration, more adsorption sites participate in the molecular adsorption process, resulting in a significant response enhancement. In particular in the case of the S2 sensor, the sensing response is very large. However, with a further increase in WO₃ concentration, the sensing response begins to decrease, which is due to the overflow film resistance. Therefore, the sensor based on S2 has the best response, that is, the best content of WO₃ is 97%. Besides, the sensitivity of the S2 sensor decreases with the increase of the working temperature. This phenomenon may be explained as follows. As the operating temperature increases to a certain extent, the number of electrons in the conduction band of WO₃ is greatly reduced, and the electron supply is insufficient to react with oxygen in the atmosphere, so that species containing oxygen ions cannot be formed. Due to the loss of oxygen-containing ions that act as active sites on the surface of the sensing materials, the reaction with 2-CEES gas becomes less, and the corresponding response is reduced.[27] The response recovery time of the S2 sensor at different operating temperatures was further calculated. The response time and recovery time of the S2 sensor toward 2-CEES gas with a concentration of 5.70 ppm at different operating temperatures are shown in Fig. 3b. It can be seen from the figure that under all operating temperatures, the response time is relatively short, within 10 s. This shows that the sensor has good responsiveness. In addition, the response time reduces as the operating temperature increases. However, when

Table 1 BET analysis results

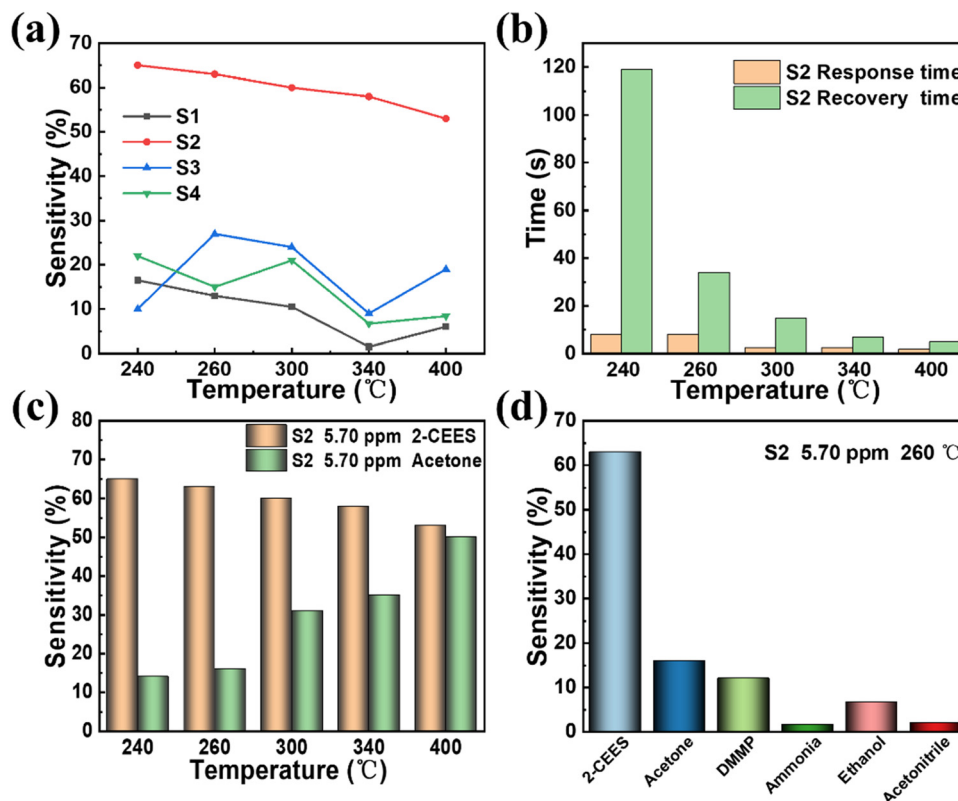| Parameter	WO₃	WO₃/graphite
a_{BET} (m² g⁻¹)	5.3456	6.1215
Total pore volume@p/p_0 = 0.990 (cm³ g⁻¹)	0.050367	0.076678

Fig. 3 Sensing performance of the WO$_3$/graphite sensor. (a) Optimization of the amount of WO$_3$ dopant and operating temperature. (b) Response time and recovery time of the WO$_3$/graphite (S2) sensor toward 5.70 ppm 2-CEES at different temperatures. (c) The sensing responses of the WO$_3$/graphite (S2) sensor toward 5.70 ppm of 2-CEES and acetone gas at different temperatures. (d) The sensing responses of WO$_3$/graphite (S2) sensor toward 5.70 ppm of 2-CEES and other gases (acetone, DMMP, ammonia, ethanol, and acetonitrile) at an operating temperature of 260 °C.

the operating temperature is low, that is, below 240 °C, the recovery time is relatively long, which is not conducive to the detection of 2-CEES gas. With the increase of operating temperature, *i.e.* higher than 240 °C and lower than 260 °C, the recovery time is significantly reduced. At the operating temperature of 260 °C, the recovery time decreases a lot to 34 s. This shows that the sensor has good recoverability. With the further increase of operating temperature, *i.e.* higher than 260 °C, the recovery time continues to decrease. Fig. 3c, Fig. S3b, and Fig. S4a (ESI†) show the sensing responses of the S2 sensor toward 5.70 ppm of 2-CEES and acetone gas at different temperatures. It can be found that when the operating temperature is 240 °C or 260 °C, the sensor has a large response toward 2-CEES gas, but the response to acetone gas is relatively small. At this time, the sensitivity of 2-CEES is almost 4 times that of acetone. As the operating temperature gets higher and higher, when it reaches 300 °C, the response of 2-CEES decreases slightly, but the response of acetone increases greatly. At this time, the response of acetone has almost reached half of that of 2-CEES. With the further increase of operating temperature, the response of 2-CEES decreases gradually, and the response of acetone further increases, and the ratio of the two responses becomes smaller and smaller. When the operating temperature reaches 400 °C, the response of acetone is almost equal to that of 2-CEES. Through the above

analysis, S2 was selected as the gas sensor material of 2-CEES, the best content of WO$_3$ is 97%, and the optimal operating temperature is 260 °C. The sensing responses of the S2 sensor toward 5.70 ppm of other interfering gases, such as acetone, DMMP, ammonia, ethanol, and acetonitrile at an operating temperature of 260 °C were also studied, as shown in Fig. 3d and Fig. S4b (ESI†). The sensor has a relatively small response toward interfering gases compared with 2-CEES gas, which indicates that the S2 sensor has good selectivity, and can detect 2-CEES in the presence of interfering gases, and has a good development prospect.

Fig. 4a displays the response time and recovery time of the S2 sensor toward 2-CEES gas with a concentration of 5.70 ppm at an operating temperature of 260 °C. It can be seen that the response time and recovery time are 8 s and 34 s, respectively. As shown in Fig. 4b, the S2 sensor can detect the 2-CEES gas with a tiny concentration of 0.10 ppm. The response-recovery curves of the S2 sensor toward 0.10, 0.31, 0.62, 0.84, 1.00, 2.10, 3.10, 4.10, 7.20, and 11.40 ppm of 2-CEES gas at an operating temperature of 260 °C are presented in Fig. 4c. The response of the S2 sensor increases with the increase of 2-CEES concentration from 0.10 ppm to 4.10 ppm, and the sensitivity increases rapidly. When the concentration of 2-CEES is greater than 4.10 ppm, the response increases slowly. This shows that the S2 sensor has a wide detection range. The linear
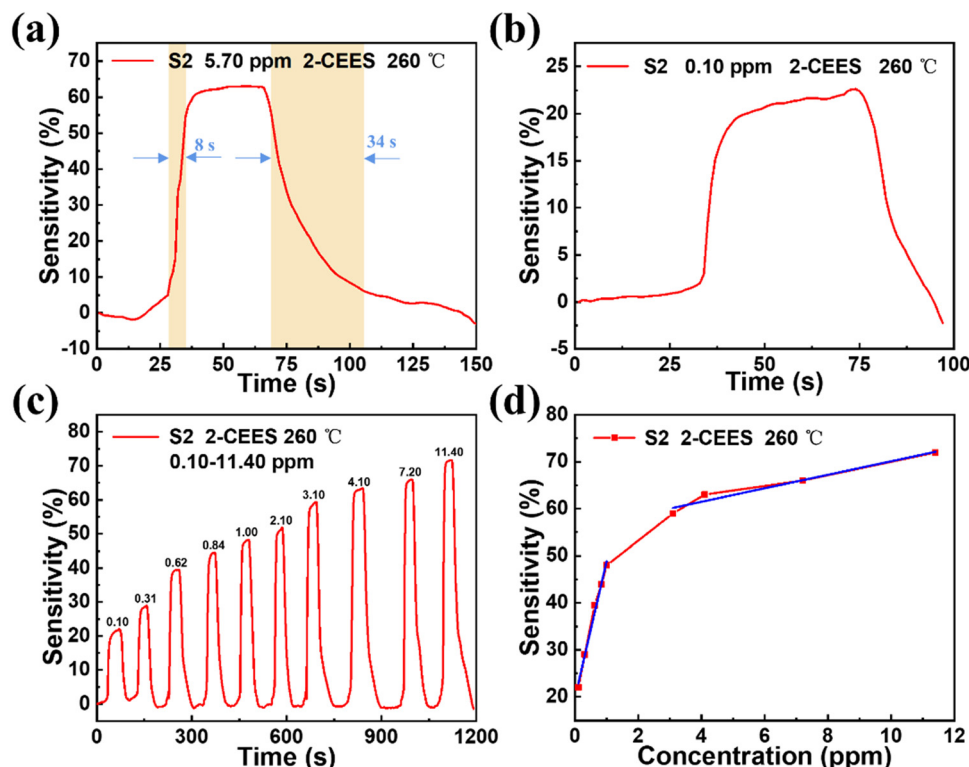
Fig. 4 Sensing performance of the WO₃/graphite (S2) sensor. (a) Response time and recovery time of the WO₃/graphite (S2) sensor for 5.70 ppm 2-CEES at an operating temperature of 260 °C. (b) The sensing responses of the WO₃/graphite (S2) sensor toward 0.10 ppm of 2-CEES at an operating temperature of 260 °C. (c) The response-recovery curves of the WO₃/graphite (S2) sensor toward 0.10, 0.31, 0.62, 0.84, 1.00, 2.10, 3.10, 4.10, 7.20 and 11.40 ppm of 2-CEES gas at an operating temperature of 260 °C. (d) The linear dependence relation of the response of the WO₃/graphite (S2) sensor toward different concentrations of 2-CEES gas at an operating temperature of 260 °C.

dependence relationship of the response of the S2 sensor toward different concentrations of 2-CEES gas at an operating temperature of 260 °C is shown in Fig. 4d.

The repeatability and long-term stability of the S2 sensor were also studied, as shown in Fig. 5. The S2 sensor has good repeatability in response to 2-CEES gas with a concentration of 5.70 ppm, and the sensitivity is almost maintained at 63%, as

shown in Fig. 5a. The long-term stability test of the S2 sensor for 2-CEES gas with a concentration of 5.70 ppm at an operating temperature of 260 °C is displayed in Fig. 5b. After 7 days of detection, the response of the sensor is also maintained at 63%, which illustrates the sensor has good long-term stability.

According to the experiment, it can be known that the concentration of 2-CEES gas has a significant impact on the
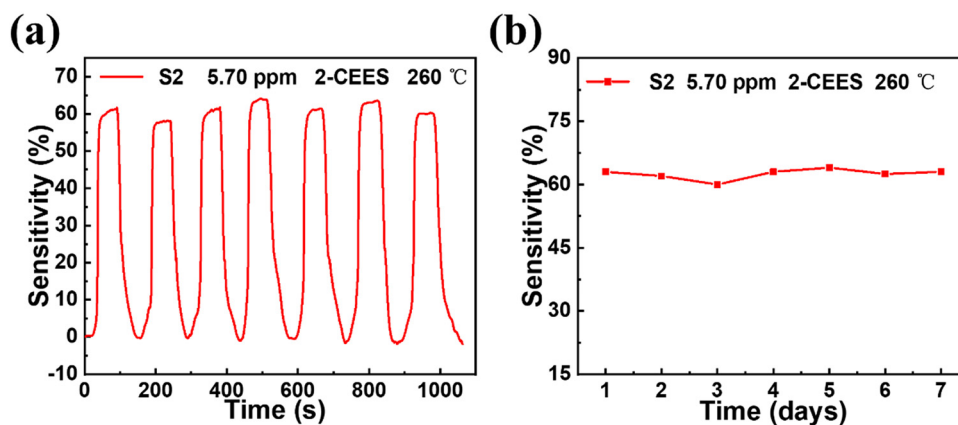

Fig. 5 Repeatability and stability test of the WO₃/graphite (S2) sensor. (a) When the operating temperature is 260 °C, the repeatability of the WO₃/graphite (S2) sensor toward 5.70 ppm 2-CEES during the seven testing cycles. (b) Long term stability of the WO₃/graphite (S2) sensor toward 2-CEES gas with a concentration of 5.70 ppm at an operating temperature of 260 °C.
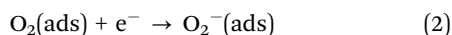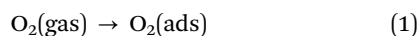
Table 2 Response time and recovery time for 2-CEES gas with various concentrations at an operating temperature of 260 °C

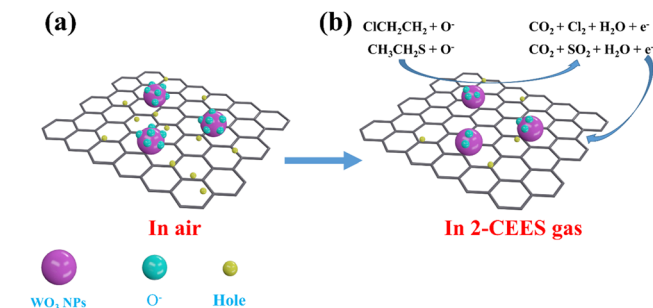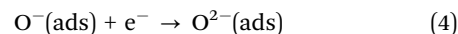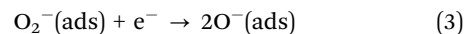| 2-CEES concentration (ppm)	Response time (s)	Recovery time (s)	Sensitivity (%)
0.10	14.5	15	22
0.84	10	25	44
4.10	9	33	63
5.70	8	34	62
11.40	6	43	72

response time and recovery time of the sensor. Table 2 shows the response time and recovery time of the S2 sensor under different concentrations of 2-CEES gas with an operating temperature of 260 °C. In this experiment, when the concentration of 2-CEES gas increases, the recovery time will increase and the response time will decrease. The response time reduction rate and recovery time extension rate were 0.752 s ppm^{-1} and 2.478 s ppm^{-1}, respectively. After comparing the performance of the S2 sensor with some studies on detecting 2-CEES gas (Table 3), it is found that the working temperature required by the sensor in this study is not high, which shows that the prepared gas sensor is energy efficient. At the same time, the sensor has a response time of 8 s and a recovery time of 34 s, which are lower than those of other sensors. These suggest that graphite doped WO$_3$ is a promising material in the application of detecting 2-CEES gas.
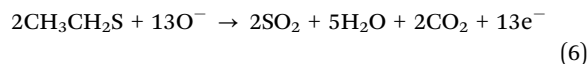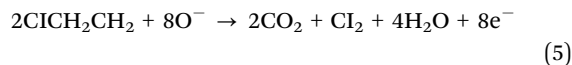
Sensing mechanism

The 2-CEES gas sensing is based on a chemiresistive process provided by the interaction of 2-CEES gas with chemisorbed oxygen on the surface of the WO$_3$/graphite, as shown in Fig. 6. When the surface of the WO$_3$/graphite sensor is exposed to air, oxygen molecules are physically adsorbed first. After absorbing activation energy, the physically adsorbed oxygen molecules are chemically adsorbed. Oxygen molecules attract electrons from the WO$_3$ conduction band, forming O$_2^-$, which increases the resistance of the WO$_3$/graphite sensor. At higher temperatures, O2− anion attracts another electron to form a 2O$^-$ anion, and the O$^-$ anion attracts another electron to form an O^{2-} anion as follows (1)–(4):

$$O_2(gas) \rightarrow O_2(ads) \tag{1}$$

$$O_2(ads) + e^- \rightarrow O_2^-(ads) \tag{2}$$

Fig. 6 Schematic diagram of the sensing mechanism of the WO$_3$/graphite sensor toward 2-CEES gas.

$$O_2^-(ads) + e^- \rightarrow 2O^-(ads) \tag{3}$$

$$O^-(ads) + e^- \rightarrow O^{2-}(ads) \tag{4}$$

As oxygen ions continue to diffuse outward, a depletion layer is formed. 2-CEES gas is a reducing gas. At a certain working temperature, when 2-CEES gas is introduced to the surface of the sensing material, the 2-CEES will quickly decompose into ClCH$_2$CH$_2$ and CH$_3$CH$_2$S. Due to the strong electrophilicity of Cl and S, oxygen ions will react quickly with it. Through the interaction of oxygen ions with ClCH$_2$CH$_2$ and CH$_3$CH$_2$S, respectively, the stripped electrons are released back to the conduction band of WO$_3$ nanoparticles, that is, the electrons are released back to the depletion layer, so as to reduce the resistance of the sensor. The reaction is as follows (5) and (6):

$$2ClCH_2CH_2 + 8O^- \rightarrow 2CO_2 + Cl_2 + 4H_2O + 8e^- \tag{5}$$

$$2CH_3CH_2S + 13O^- \rightarrow 2SO_2 + 5H_2O + 2CO_2 + 13e^- \tag{6}$$

For nanocomposites containing graphite, graphite inhibits the agglomeration of WO$_3$ nanoparticles, which increases the specific surface area of WO$_3$ nanoparticles.[28] Moreover, the porous structure of WO$_3$/graphite is conducive to the diffusion of oxygen molecules and 2-CEES gas, which increases the surface reactive sites of the sensing material, thereby improving the performance of the sensor.[29]

Conclusion

In conclusion, the sensing properties of WO$_3$/graphite nanocomposites prepared by simple blending for 2-CEES gas were studied. The results show that the sensing performance of WO$_3$/graphite hybrid materials is better compared with pure WO$_3$ materials, and when the WO$_3$ mass fraction is 97%, the gas sensor exhibits the best performance. The gas sensor has a 63% response toward 5.70 ppm 2-CEES at an operating temperature of 260 °C, a rapid response/recovery time (8 s/34 s), and excellent reproducibility, long-term stability and selectivity. Based on the above results and discussions, the detection of

Table 3 Comparison of the 2-CEES sensor performances in this research with recent studies

Sensing material	2-CEES (ppm)	Temperature (°C)	Response time (s)	Recovery time (s)	Ref.
WO$_3$/graphite	5.70	260	8	34	This work
Pt-CdSnO$_3$	4	300	8	125	25
Ru-CdSnO$_3$	4	350	5	185	24
ZnO NPs	1	250	34	—	30
Al-doped ZnO NPs	20	500	10	400	26
Al-doped ZnO QDs	20	450	3	406	14
Sm$_2$O$_3$ doped SnO$_2$	10	200	50	20	31

dichlorodiethyl sulfide based on the WO_3/graphite gas sensor has good development prospects.

Author contributions

C. Q., K. L. and W. Y. conceived the idea, performed the experiments and drafted the manuscript. W. Z. and Y. F. participated in the results discussion. C. X. and C. S. helped with the characterization analysis. S. W. reviewed and revised the manuscript.

Conflicts of interest

The authors declare no competing financial interest.

Acknowledgements

References

1 S. Chauhan, R. D'cruz, S. Faruqi, K. Singh, S. Varma, M. Singh and V. Karthik, *Environ. Toxicol. Pharmacol.*, 2008, **26**, 113–122.

2 K. Kim, O. G. Tsay, D. A. Atwood and D. G. Churchill, *Chem. Rev.*, 2011, **111**, 5345–5403.

3 K. Ganesan, S. Raza and R. Vijayaraghavan, *J. Pharm. BioAllied Sci.*, 2010, **2**, 166.

4 Y. Fan, K. Li, X. Ren, W. Yan, C. Zhu, Y. Zhao, W. Zeng, Z. Chen and S. Wang, *J. Mater. Chem. C*, 2021, **9**, 17496–17503.

5 C. Karnati, H. Du, H.-F. Ji, X. Xu, Y. Lvov, A. Mulchandani, P. Mulchandani and W. Chen, *Biosens. Bioelectron.*, 2007, **22**, 2636–2642.

6 R. C. Thomas, H. C. Yang, C. R. DiRubio, A. J. Ricco and R. M. Crooks, *Langmuir*, 1996, **12**, 2239–2246.

7 R. A. McGill, V. K. Nguyen, R. Chung, R. E. Shaffer, D. DiLella, J. L. Stepnowski, T. E. Mlsna, D. L. Venezky and D. Dominguez, *Sens. Actuators, B*, 2000, **65**, 10–13.

8 D. D. Dominguez, R. Chung, V. Nguyen, D. Tevault and R. A. McGill, *Sens. Actuators, B*, 1998, **53**, 186–190.

9 G. M. Milner, 2005.

10 C. Zimmermann, P. Mazein, D. Rebiere, C. Dejous, J. Pistre and R. Planade, *IEEE Sens. J.*, 2004, **4**, 479–488.

11 W. P. Carey and B. R. Kowalski, *Anal. Chem.*, 1986, **58**, 3077–3084.

12 O. S. Milanko, S. A. Milinković and L. V. Rajaković, *Anal. Chim. Acta*, 1992, **269**, 289–300.

13 S.-W. Zhang and T. M. Swager, *J. Am. Chem. Soc.*, 2003, **125**, 3420–3421.

14 J. H. Lee, H. Jung, R. Yoo, Y. Park, H.-S. Lee, Y.-S. Choe and W. Lee, *Sens. Actuators, B*, 2019, **284**, 444–450.

15 S. M. Kanan, A. Waghe, B. L. Jensen and C. P. Tripp, *Talanta*, 2007, **72**, 401–407.

16 D. C. Meier, C. J. Taylor, R. E. Cavicchi, M. Ellzy, K. Sumpter and S. Semancik, *IEEE Sens. J.*, 2005, **5**, 712–725.

17 Y. Hu, T. Li, J. Zhang, J. Guo, W. Wang and D. Zhang, *Sens. Actuators, B*, 2022, **352**, 130912.

18 D. Zhang, Y. Cao, J. Wu and X. Zhang, *Appl. Surf. Sci.*, 2020, **503**, 144063.

19 D. Wang, D. Zhang, J. Guo, Y. Hu, Y. Yang, T. Sun, H. Zhang and X. Liu, *Nano Energy*, 2021, **89**, 106410.

20 S. Yu, D. Zhang, Y. Zhang, W. Pan, B. E. Meteku, F. Zhang and J. Zeng, *Nanoscale*, 2020, **12**, 18815–18825.

21 D. Zhang, Z. Yang, S. Yu, Q. Mi and Q. Pan, *Coord. Chem. Rev.*, 2020, **413**, 213272.

22 D. Zhang, Y. Cao, Z. Yang and J. Wu, *ACS Appl. Mater. Interfaces*, 2020, **12**, 11979–11989.

23 Y. H. Park, H.-K. Song, C.-S. Lee and J.-G. Jee, *J. Ind. Eng. Chem.*, 2008, **14**, 818–823.

24 L. Patil, V. Deo, M. Shinde, A. Bari, D. Patil and M. Kaushik, *Sens. Actuators, B*, 2014, **191**, 130–136.

25 L. Patil, V. Deo, M. Shinde, A. Bari and M. Kaushik, *Sens. Actuators, B*, 2011, **160**, 234–243.

26 R. Yoo, D. Lee, S. Cho and W. Lee, *Sens. Actuators, B*, 2018, **254**, 1242–1248.

27 R. Mishra, S. Upadhyay, A. Kushwaha, T.-H. Kim, G. Murali, R. Verma, M. Srivastava, J. Singh, P. Sahay and S. H. Lee, *Nanoscale*, 2015, **7**, 11971–11979.

28 A. Singh, A. Sharma, M. Tomar and V. Gupta, *Sens. Actuators, B*, 2017, **245**, 590–598.

29 C. A. Zito, T. M. Perfecto and D. P. Volanti, *Sens. Actuators, B*, 2017, **244**, 466–474.

30 R. Yoo, C. Oh, M.-J. Song, S. Cho and W. Lee, *J. Nanosci. Nanotechnol.*, 2018, **18**, 1232–1236.

31 H. M. Aliha, A. A. Khodadadi and Y. Mortazavi, *Sens. Actuators, B*, 2013, **181**, 637–643.